Optical Materials 84 (2018) 722–727

Contents lists available at ScienceDirect

Optical Materials

journal homepage: www.elsevier.com/locate/optmat

Design and fabrication of composite structures in ZnSe providing broadband mid-infrared anti-reflection

Liang Fei[a,b], Yun Cui[a,*], Dongyun Wan[b,**], Yuanan Zhao[a], Meiping Zhu[a], Yunxia Jin[a], Kui Yi[a], Jianda Shao[a]

[a] Laboratory of Thin Film Optics, Key Laboratory of Materials for High Power Laser, Shanghai Institute for Optics and Fine Mechanics, Chinese Academy of Sciences, Shanghai, 201800, China
[b] School of Materials Science and Engineering, Shanghai University, Shanghai, 200444, China

ARTICLE INFO

Keywords:
Anti-reflection
ZnSe
Finite-difference time-domain
Mid-infrared

ABSTRACT

A comparative study of anti-reflection microstructures (ARMs) and ARMs with Al_2O_3 coatings (Al_2O_3/ARMs) on zinc selenide (ZnSe) has been carried out. The transmittance and electric field intensities were analyzed and presented using finite-difference time-domain (FDTD) simulations. ARMs were successfully fabricated on ZnSe surfaces by reactive ion etching and an Al_2O_3 layer was deposited onto the ARMs by an ion beam sputtering method. The theoretical analysis and experimental results showed that the transmittance of Al_2O_3/ARMs-treated ZnSe had a close relationship with the thickness of Al_2O_3 layer and was higher than that of ARMs-treated ZnSe in the 2–5 μm wavelength range, which was due to the fact that the Al_2O_3/ARMs had a better graded refractive index profile. The angle-dependent reflectance of ZnSe with Al_2O_3/ARMs was lower than that with ARMs. A difference of the spatial distribution of the electric field intensity between ARMs and Al_2O_3/ARMs was observed due to the surface Al_2O_3 coating, which predicted qualitative laser damage thresholds for both structures. The results of this study provide potential applications in high-efficiency IR optoelectronic devices and high power mid-infrared laser systems.

1. Introduction

ZnSe is one of the most important materials with prominent applications in many optical components, such as windows and lenses [1], as well as in solar cells [2], lighting phosphors [3], LEDs and infrared lasers when appropriately doped [4–7]. It provides excellent transmission in the visible and IR regions (0.45–20 μm) due to its wide bandgap [8]. However, because of its high refractive index (n = 2.67 @ 0.55 μm, n = 2.40 @ 10.6 μm), the average transmittance of optical windows and lenses made of ZnSe is less than 70% [9]. As a result, high performance anti-reflective coatings (ARCs) are often required for ZnSe substrates and components [10,11], but the precise control requirements for each layer thickness in multilayer coatings, the limited selection of materials appropriate to different IR wavelength bands and various substrates, and the poor environmental stability caused by the mismatch of the thermal expansion coefficients between materials greatly impeded their design and fabrication. Laser induced damage thresholds (LIDTs) that are low, and the lack of durability of traditional anti-reflection (AR) coatings for mid-infrared bands should not be ignored [12–15].

Studies on biomimetic subwavelength structures, originally inspired by insect compound eyes, have been developed as antireflective surfaces that exhibit promising broadband and quasi-omnidirectional antireflective properties [16]. In recent years, various nanofabrication techniques have emerged. Unfortunately, reported works mostly focused on fabricating and characterizing moth-eye AR surfaces operating at visible and near-IR wavelength ranges [17–19]. Mid-infrared regions were typically not addressed due to their relatively wide wavelength range and the technical difficulties in fabricating the required antireflection structures with high aspect ratios.

Previous studies mostly focused on fabricating and characterizing ARMs-treated ZnSe with a high aspect ratio for the mid-infrared range [20–23]. Random moth-eye (RM) surface structures with high aspect ratio (approximately 5) were produced on ZnSe optical components for mid-infrared wavelengths [22]. Periodic arrays of hexagonally close-packed conical frusta (pitch = 690 nm, height = 2800 nm) were fabricated on ZnSe, yielding a single-side average transmission improvement compared to a flat surface, 78% compared to 68%, over a large infrared

* Corresponding author.
** Corresponding author.
E-mail addresses: cuiyun@siom.ac.cn (Y. Cui), echowandy@shu.edu.cn (D. Wan).

https://doi.org/10.1016/j.optmat.2018.08.010
Received 13 May 2018; Received in revised form 1 August 2018; Accepted 5 August 2018

bandwidth [23]. Hence, there is a need to design and fabricate excellent mid-infrared anti-reflectivity for ZnSe with an appropriate aspect ratio.

In this report, we present composite broadband mid-infrared ARMs on ZnSe substrates with a reasonable aspect ratio. The geometry and pitch length of the ARMs were optimized to maximize their transmittance over a wide wavelength range, 2–5 μm. For further improving the optical characteristics, the effects of a low-refractive index Al_2O_3 layer deposited onto the ARMs were studied as a possible route to reducing the aspect ratio design requirement. Furthermore, pertinent optical characteristics were theoretically and experimentally analyzed using finite-different time-domain (FDTD) simulation.

2. Design and experimental methods

The electromagnetic behavior of ARMs and Al_2O_3/ARMs were analyzed using the *Lumerical FDTD Solution* software [24], which implements the FDTD algorithm to model the propagation of electromagnetic radiation through sub-wavelength scale structure by numerically solving Maxwell's equations. Before designing and optimizing the thickness of the Al_2O_3 layer on ARMs-treated ZnSe substrates for broadband and high anti-reflectivity, the geometry of ARMs on ZnSe needed to be theoretically explored. In this work, ARMs consisting of a squarely close-packed conical frusta array with a spacing of 800 nm was chosen because the incident wavelength range of interest is 2–5 μm at 0°incident angle; the feature spacing should be less than λ/n_s to avoid diffraction effects in transmission area, where λ is the minimum wavelength of operation and n_s is the refractive index of the substrate [25].

The simulation domain for FDTD calculations consisted of squarely close-packed conical frusta in the *x*-*y* plane, as depicted in Fig. 1. The simulated substrate model has a geometry of ARMs as follows: spacing = 800 nm, width = 800 nm, height = 1000 nm. The Al_2O_3/ARMs model is the same as the ARMs simulated model; its height becomes large corresponding to the thickness increase of the layer, which implies Al_2O_3 is deposited uniformly onto the surface of the ARMs-treated substrate. Periodic boundary conditions were used in both *x*- and *y*-directions to represent the periodic surface structure. The perfectly matched layer (PML) approach was used at the top and bottom of the simulated area for providing absorption boundary conditions. A plane wave source (λ = 2–5 μm) with wave vector *k* in the –*z* direction was set close to the upper boundary. The transmitted field was recorded with a field monitor below the surface. The electric fields of *x*-slice and *y*-slice were respectively recorded with *y*-*z* field monitor and *x*-*z* field monitor. Material properties of ZnSe and the Al_2O_3 film were based on Lumerical software-generated fits to literature data [26,27]. It can be shown, for a circularly symmetric three-dimensional microstructure in a square or hexagonal packing scheme, such as the structures we study here, that there should be no dependence on polarization if the incident light is normal to the surface [28]. Therefore, in the present work, it is sufficient to study a single polarization with the plane of the incoming electric field set in *x*-*z* plane.

The transmittances over a range of wavelengths and for different thicknesses of the Al_2O_3 layer (T_{Al2O3}) in Al_2O_3/ARMs was calculated as shown in Fig. 2. Fig. 2(a) shows the contour plot of the calculated transmittance as a function of wavelength and thickness. We assumed that the Al_2O_3 was deposited homogeneously along the vertical and lateral directions. As shown in Fig. 2(a), the modelled transmittance considerably increased with the increase of the T_{Al2O3} between 3.5 and 5 μm. However, at wavelengths less than 3.5 μm, the transmittance is decreased with slight fluctuations. Fig. 2(b) reveals that the average transmittance over 2–5 μm gradually increases with the thickness of the Al_2O_3 layer from zero to 350 nm but decreases with further increase of the T_{Al2O3}. This means that an appropriate (Al_2O_3 layer thickness) T_{Al2O3} can assist in the improvement of the transmittance of ARMs-treated ZnSe. The transmittance of composite ARMs are enhanced by the higher graded-refractive index profile along the light incident direction, i.e., the low-refractive index Al_2O_3 layer acts as the intermediate-refractive index layer between air and the surface of ARMs-treated ZnSe.

To fabricate single-side ARMs on ZnSe substrates, double-side polished 3-mm thick ZnSe substrates were used. After an interferometric lithography process, the squarely-arrayed pattern was generated. The squarely close-packed conical frusta structure array was prepared through reactive ion etching, where the feature spacing was about 800 nm and height was about 1000 nm. Next, the Al_2O_3 layer (350-nm thickness) was deposited on the substrate by ion beam sputtering. The transmission characteristics of the ZnSe substrates with ARMs and Al_2O_3/ARMs were measured in air using a Nicolet 6700 Fourier transform infrared (FTIR) spectrometer employing a liquid-nitrogen-cooled mercury cadmium telluride detector. For accurate analysis of the surface structures, we used scanning electron microscopy (SEM) as well as focused ion-beam (FIB) milling. The latter technique was required in order to evaluate the depth of a given feature. An ion beam was used to mill out portions of the material, revealing a cross-section in the feature.

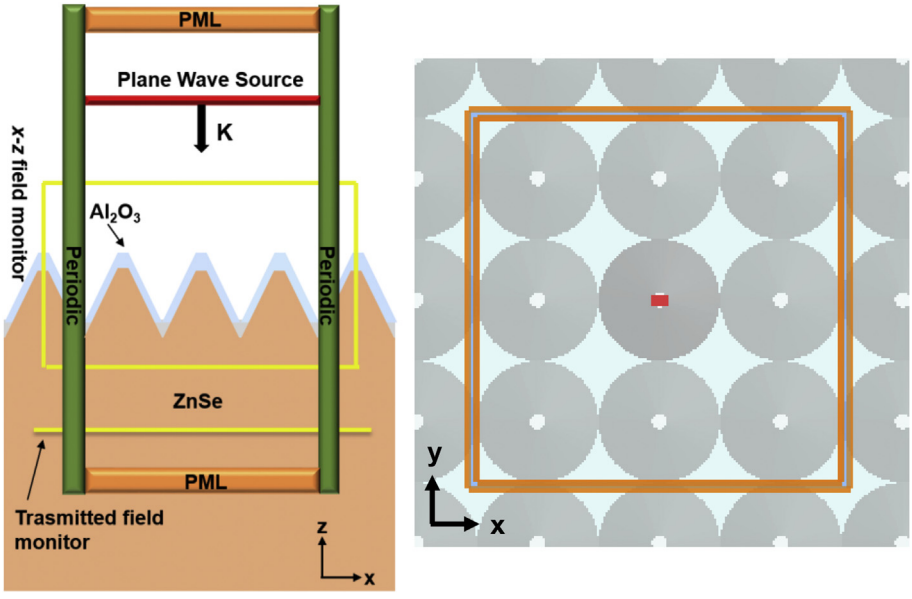

Fig. 1. FDTD model and simulation domain for microstructure substrates.